remote sensing

MDPI

Article

Solar Extreme and Far Ultraviolet Radiation Modeling for Aeronomic Calculations

Anatoliy A. Nusinov *, Tamara V. Kazachevskaya and Valeriya V. Katyushina

Fedorov Institute of Applied Geophysics (IAG), 129128 Moscow, Russia; Kazachevskaya@mail.ru (T.V.K.); katyushina@bk.ru (V.V.K.)

* Correspondence: nusinov@mail.ru

Abstract: Modeling the upper atmosphere and ionospheres on the basis of a mathematical description of physical processes requires knowledge of ultraviolet radiation fluxes from the Sun as an integral part of the model. Aeronomic models of variations in the radiation flux in the region of extreme (EUV) and far (FUV) radiation, based mainly on the data of the last TIMED mission measurements of the solar spectrum, are proposed. The EUVT model describes variations in the 5–105 nm spectral region, which are responsible for the ionization of the main components of the earth's atmosphere. The FUVT model describes the flux changes in the 115–242 nm region, which determines heating of the upper atmosphere and the dissociation of molecular oxygen. Both models use the intensity of the hydrogen Lyman-alpha line as an input parameter, which can currently be considered as one of the main indices of solar activity and can be measured with relatively simpler photometers. A comparison of the results of model calculations with observations shows that the model error does not exceed 1–2% for the FUVT model, and 5.5% for EUVT, which is sufficient for calculating the parameters of the ionosphere and thermosphere.

Keywords: sun; solar extreme ultraviolet radiation; far ultraviolet radiation; radiation models

Citation: Nusinov, A.A.; Kazachevskaya, T.V.; Katyushina, V.V. Solar Extreme and Far Ultraviolet Radiation Modeling for Aeronomic Calculations. *Remote Sens.* **2021**, *13*, 1454. https://doi.org/10.3390/rs13081454

Academic Editor: Loredana Perrone

Received: 2 March 2021
Accepted: 3 April 2021
Published: 9 April 2021

1. Introduction

Extreme and far ultraviolet radiation is the most significant of the entire solar spectrum for the formation and composition of the ionosphere and upper atmosphere. The impact of radiation on the upper atmosphere leads to a number of photochemical processes, which are mainly made up of ionization and dissociation of atmospheric gas molecules. The origination of atomic oxygen is due to the dissociation of oxygen molecules under the influence of ultraviolet radiation and transfer processes. The dissociation threshold corresponds to the radiation wavelength $\lambda = 242$ nm [1]. At altitudes of more than ~120 km, the concentrations of atomic and molecular oxygen become equal, and at altitudes of ~180 km, the concentration of atomic oxygen also exceeds the concentration of nitrogen molecules, and atomic oxygen becomes the main component of the upper atmosphere (e.g., [2]). At wavelengths shorter than 104 nm, atmospheric gases are ionized (see, for example, [2]). For this part of the spectrum, the production of oxygen atoms can be neglected. In addition to dissociation, absorption in the atmosphere by FUV leads to its heating (see, for example, [3]). The thermosphere and ionosphere are influenced by the joint efforts of solar radiation, geomagnetic activity and the lower atmosphere forcing. All these terms play important roles in the distribution of the thermosphere and ionosphere composition. The importance of taking into account variations in the flux of UV radiation with the level of activity in the study of the upper atmosphere was emphasized by Mterkel et al. [4]: if during the transition from the minimum solar activity to the maximum, the temperature changes at an altitude of ~10 km is ~0.1 K, and ~1 K by 50 km, then at altitudes of ~500 km, in the thermosphere, the changes exceed 400 K. Thus, to model the main processes of the formation of the upper atmosphere and ionosphere, knowledge of solar radiation fluxes in the region of 10–242 nm is required. Ultimately, long-term changes in the upper atmosphere

are due to variations in this range. Modeling the spectrum of solar ultraviolet radiation is an important integral task of a number of other problems, such as the effect of radiation on the surface of spacecraft, problems of space materials science. or changes in atmospheric ozone (e.g., [4]). Simulation of FUV fluxes under various heliophysical conditions is essential for solving some practical problems arising in the development of space technology. In particular, it is necessary to take into account the factors of influence that lead to the degradation of various components of spacecraft, and are determined, along with the fluxes of ultraviolet radiation, for example, photoelectrons, fluxes of oxygen ions O^+, and other charged particles of low energy, the characteristics of which are due to the state of the upper atmosphere. The actual issue is the problem of "atmospheric subsidence" i.e., the existence of a systematic decrease in the density of the upper atmosphere at fixed altitudes (see, for example, [5]). One of the possible mechanisms of such a change is a decrease in the intensity of heating of the atmosphere and the rate of dissociation of molecular oxygen due to a decrease in the FUV flux.

Models of the solar extreme ultraviolet (EUV) and far ultraviolet (FUV) spectra are used to quickly determine the characteristics of the near-Earth space environment, subject to adaptation to data from ground-based and space-based monitoring facilities. The radiation model makes it possible to trace long-term variations in the FUV using archived data on input parameters for a long time exceeding the duration of the epoch of satellite observations, for example, using ionospheric data [6].

Despite the urgency of the problem of creating a sufficiently accurate and easily used model of FUV radiation, which adequately describes both the magnitudes of the radiation fluxes and their variations for different time scales, there are still no models that reliably reproduce the radiation fluxes in this range at different levels of solar activity. There is a reference spectrum for the 2008 minimum of activity [7], methods for calculating the spectrum for wavelengths from 200 nm were proposed [8–10]. The NRLSSI [9] and SATIRE [11] models, in principle, satisfy the above requirements. However, it is difficult to use them. This is because it requires simultaneous observation of sunspots, flare areas, and Mg-index. In addition, Merkel et al. noted [12] that the NRLSSI model gives significantly underestimated results in comparison with reliable measurements onboard SORCE mission.

When developing EUV models [13–16], relatively small datasets were used, often from different sources, which led to an additional loss of accuracy. It can be expected that the existing models used in the tasks of monitoring the geophysical environment can be noticeably improved due to the emergence of new data over the past decades. The direction of improving predictive models is to use data from monitoring the Sun and the interplanetary medium by ground-based observatories and space vehicles.

Along with the change in the volume of the initial data, the set of control parameters of the models has also changed significantly recently. Currently, in the EUV models, along with ground-based measurements (as a rule, radio fluxes at a wavelength of 10.7 cm, F10.7, as, for example, in the EUVAC model [15]), the results of observations on spacecraft are used. These are, for example, models EUV-81 [16], FISM [17,18], and SOLAR2000 [19], with several intensities of spectral lines as control parameters, or the magnesium index is used, with the ratio of intensities in the core and wings of the MgII line at wavelengths near 280 nm [20]. The possibility of combining spectral measurements in the FUV region with the MgII index [21], or the "color index" [22], which changes in time like the MgII index, is being considered. It was noted [23] that different measurements of the MgII index contradict each other and, like other indices, require correction. The flux in the 58.4 nm He II line is used as an index of solar activity for calculating the spectrum of ultraviolet radiation [13,14],. Thus, it turns out that in order to use modern models of EUV radiation for monitoring space weather, it is necessary to measure the intensity in several lines or parts of the spectrum in the EUV region with a spectral resolution of no worse than 0.1 nm.

At present, it is difficult to hope for the implementation of such measurements in the monitoring mode due to their technical complexity and high cost. As an alternative to spectral measurements, it is possible to propose monitoring the EUV radiation by simpler

and cheaper means, i.e., narrow-band photometers, which select a narrow part of the spectrum in the EUV region. The photon flux in the 121.6 nm region (Lα, Lyman-alpha hydrogen line) seems to be the most suitable for this purpose. Accordingly, using existing models, they must be modified to accommodate Lα measurements as input parameters.

The EUV model [13,14] is based on the property of the spectrum in the EUV region, that the ratio R_λ of the intensities of most lines and spectral intervals to the intensity of the HeI reference line with a wavelength of λ = 58.4 nm varies slightly with the solar activity level (except for a few coronal lines). The aim of this work is to develop models of the extreme (EUV) and far (FUV) ultraviolet radiation fluxes of the quiet (in the absence of flares) Sun in the wavelength range from 10 to 105 nm (EUV) and 115–242 nm (FUV), using as input parameters the results of measurements of the solar radiation flux in the Lyman-alpha line, received from the space segment of the geophysical monitoring system. It is proposed to use these models as a future space weather monitoring tool based on monitoring the radiation in the Lα line using spectral-selective photometers installed on geostationary satellites.

2. Source Data

2.1. EUV Data

It can be expected that the existing models for use in monitoring geophysical conditions can be noticeably improved due to the emergence of new data over the past 30 years. Time series of measurements obtained from satellites differ in both the spectral range, observation period, measurement duty cycle, and accuracy, calibration, and a number of other parameters.

When developing an empirical-statistical model, it is necessary that the data used satisfy a number of requirements. First, their variations should correspond to the widest range of levels of solar activity, from minimum to maximum. The data should be obtained with the same instrument during the solar cycle or over a longer period. However, with long-term measurements, the sensitivity of the instruments can change significantly due to degradation of the sensors (see, for example, [24–26]).

At the same time, it is difficult to distinguish long-term changes caused by solar activity in time series from the effects of degradation of measuring instruments. It should be noted that the change in sensitivity with time can be nonmonotonic, as was observed, for example, in measurements by the VUSS instrumentation onboard the CORONAS-F spacecraft [27]. Elimination of degradation effects is possible by using in-flight calibration, comparing current data with calibration measurements on rockets or with reference (gas-discharge lamps or stars) sources. Recently, it has been possible to eliminate the effects of hardware degradation with the help of improved data analysis methods [25].

Currently, the most detailed EUV spectra in the region shorter than 105 nm are systematically observed on the TIMED (Thermosphere-Ionosphere-Mesosphere Energetics and Dynamics) spacecraft. To create the model, we used long-term observations of the solar spectra in the short-wave ultraviolet region of 26–195 nm, carried out during 2002–2021. Equipment SEE (Solar Extreme Ultraviolet Experiment) includes the spectrometer EGS (EUV Grating Spectrograph), and the device XPS-XUV Photometer System- “System of X-ray and ultraviolet photometers “. EGS instruments (spectrograph with a diffraction grating) measure in the wavelength range of 27–194 nm with a resolution of 1 nm, and XPS instruments cover the wavelength range 0.1–27 nm and use silicon photodiodes and filters as X-ray detectors [28]. The data of observations by the SEE equipment for each day are posted on the Internet on the TIMED spacecraft website. At present, this spacecraft is, in essence, the only source of daily data on the solar spectrum in the EUV region.

2.2. FUV Data

At present, a large amount of data from satellite observations of solar radiation fluxes in the FUV spectrum region has been accumulated. The data obtained within the SORCE (Solar Radiation and Climate Experiment, 2003 to date) and TIMED, (2002 to the present

time) are the most reliable, covering the entire solar cycle in time. The SORCE spectral range (115–308 nm) fully includes all wavelengths corresponding to the developed model, while the TIMED range (27–190 nm) contains only a part of the specified range. Based on this, the SORCE measurement data were taken to develop the model, and the TIMED data were used to validate the model. It should be noted that this use of the data is justified since the same calibration methods were used in both projects.

2.3. Lyman Alpha Data

There is a question about which time series which time series Lα to choose for building models. In particular, the longest and most accessible continuous series are the Lyman-alpha (Lα composite, hereinafter LαC) composite series [29] and the TIMED (LαT) measurement series. The LαC series, based on satellite measurements and ground-based observatory data, presents daily Lyman α values starting in 1947, spanning nearly seven solar cycles. Several versions of the Lα Composite are presented on the Internet in different years due to expansion, data revision and calibration refinement. An improved and revised version 4 is currently recommended [29]. The LαC data series, with daily updates, is available at https://lasp.colorado.edu/lisird/data/composite_lyman_alpha/ (2 March 2021). These data are presented in Figure 1. The dotted lines represent the 81-day moving average. It can be seen from the figure that the composite data (LαC, that includes both measurements on various spacecrafts and model calculations using the MgII-index) and the data of direct measurements (LαT) onboard TIMED spacecraft, change in time in a similar way, and LαC systematically exceeds LαT.

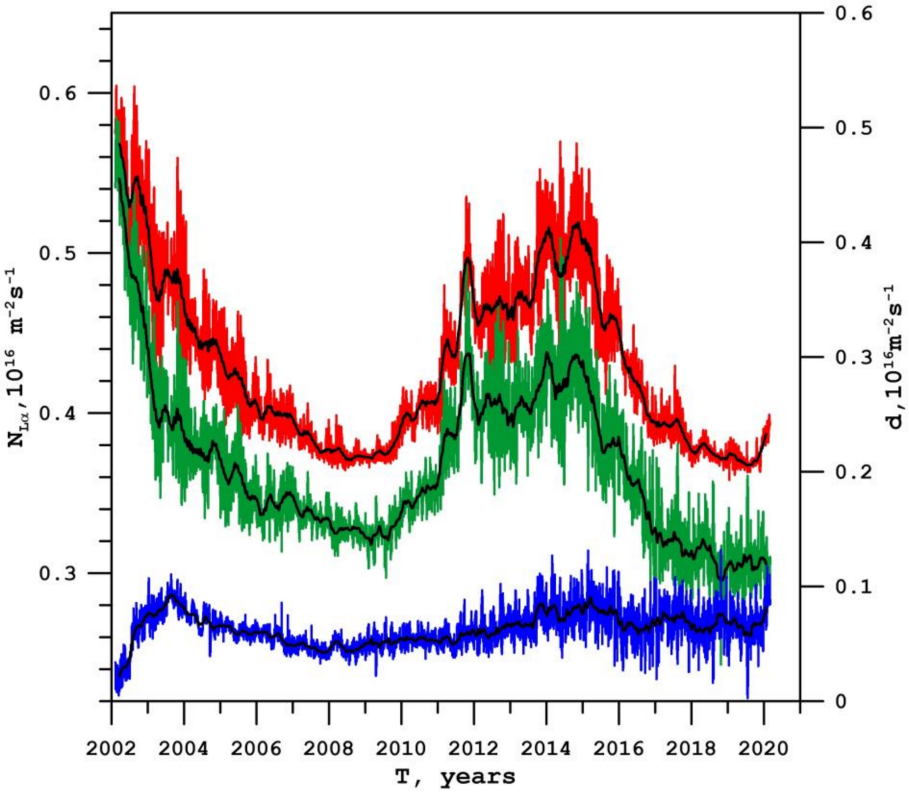

Figure 1. Changes in LαC (**red**) and LαT (**green**) in 23 and 24 cycles of activity. (**Blue**)—difference d between data. Color lines correspond to daily data. Black lines represent 81-day moving averages.

It should be noted that practically the same LαC values correspond to the minima of cycles 23–24 and 24–25, while for LαT the values at the activity minima differ by almost 7%. This is apparently caused by the degradation of the SEE hardware on TIMED. Figure 1 shows also the time variation of the difference *d* between the composite series and the

data measured. It can be seen that the difference between the intensities of LαC and LαT increases noticeably, and then, starting from 2005, fluctuates around a certain average value of ~1 mW·m^{-2}, which is most likely caused by a decrease in the sensitivity of the SEE equipment. An alternative reason may be a systematic decrease in the flux of extreme ultraviolet radiation during the epoch of a decline in solar activity during the 24th solar cycle. However, this hypothesis is contradicted by the behavior of LαC, which corresponds to the equality of fluxes at the epochs of minimum solar activity, typical for time series of EUV.

When developing the model, the index N (LαC) was chosen, which will allow the reconstruction of the EUV and FUV spectra from 1947. Nevertheless, current measurements on TIMED can be used for estimates, since the intensities of LαC and LαT are closely related to each other as can be seen in Figure 1. If it is necessary to replace one of the indices with another, the replacement can be performed using the ratio obtained from the regression analysis of the corresponding time series:

$$N\ (LaT) = 0.865\ N\ (LaC), \quad (1)$$

where N is the photon flux density in units of 10^{15} m^{-2}s^{-1}.

3. Results

3.1. EUVT Model

It is assumed that the model will be used primarily for calculating the parameters of the ionosphere and various effects associated with changes in the fluxes of EUV-radiation. Therefore, it will accept a set of lines and spectral intervals included in the EUVAC model [15], which is often used in solving problems of aeronomy.

Bruevich and Nusinov [13] proposed for calculating the spectrum in the range 10–105 nm, to use the He I λ = 58.4 nm line as a reference and considered the ratio

$$R_\lambda = N_\lambda / N_{\lambda r}. \quad (2)$$

where N_λ is the flux of quanta for a line with a wavelength λ, $N_{\lambda r}$ is the flux in the reference line, considered as an index of solar activity.

Based on the analysis of measurement data on the AE-E satellite and earlier measurements, it was shown [13] that R_λ for lines with ionization temperatures differing even by 2 orders of magnitude changes little in the solar cycle and can be represented in decomposition by activity index $N_{\lambda r}$:

$$R_\lambda = B0_\lambda + B1_\lambda N_{\lambda r}, \quad (3)$$

where $B0_\lambda$ and $B1_\lambda$ are coefficients for each of the lines or spectral intervals with a wavelength λ. Equations (2) and (3) correspond to quadratic dependence of N_λ on $N_{\lambda r}$:

$$N_\lambda = N_{\lambda r} \cdot (B0_\lambda + B1_\lambda N_{\lambda r})$$

According to the data of various experiments, the values of $B0_\lambda$ and $B1_\lambda$ were determined for the range 10–105 nm. Comparison of calculation results with measurements shows a good agreement (error < 10%) in all spectral intervals.

It can be assumed that to solve this problem, it is advisable to apply the methodology of [13] using TIMED/SEE data and daily data of the Lα line intensity.

The division of the spectrum into separate wavelength intervals is performed in EUV model similarly to that used in the models [13,15,16].

When passing to a new reference line of the spectrum, it is additionally necessary to check the property of low variability R_λ for a new index—the flux in the Lα line. The ratio R_λ was considered on the basis of the TIMED/SEE measurement database and using the data on the intensity of the LαC composite line for the period 2002–2017, which included sections of 23–24 cycles of solar activity, corresponding to the minimum of 23–24 cycles,

phases of growth and decline of activity and the maximum of the 24th cycle. It is significant that, starting from 2017, for a number of lines, a sharp increase in R_λ appears with a decrease in the N(LαT) intensity, which indicates the probable appearance of failures in the operation of the equipment, or a possible revision of the calibration, which was indirectly indicated by Woods et al. [25]. Therefore, the time series used were limited to 2017.

Changes in the R_λ values depending on the flux in the Lα line during this period are shown in Figure 2 for several lines. It can be seen that the changes in R_λ are indeed small for almost all levels of solar activity considered.

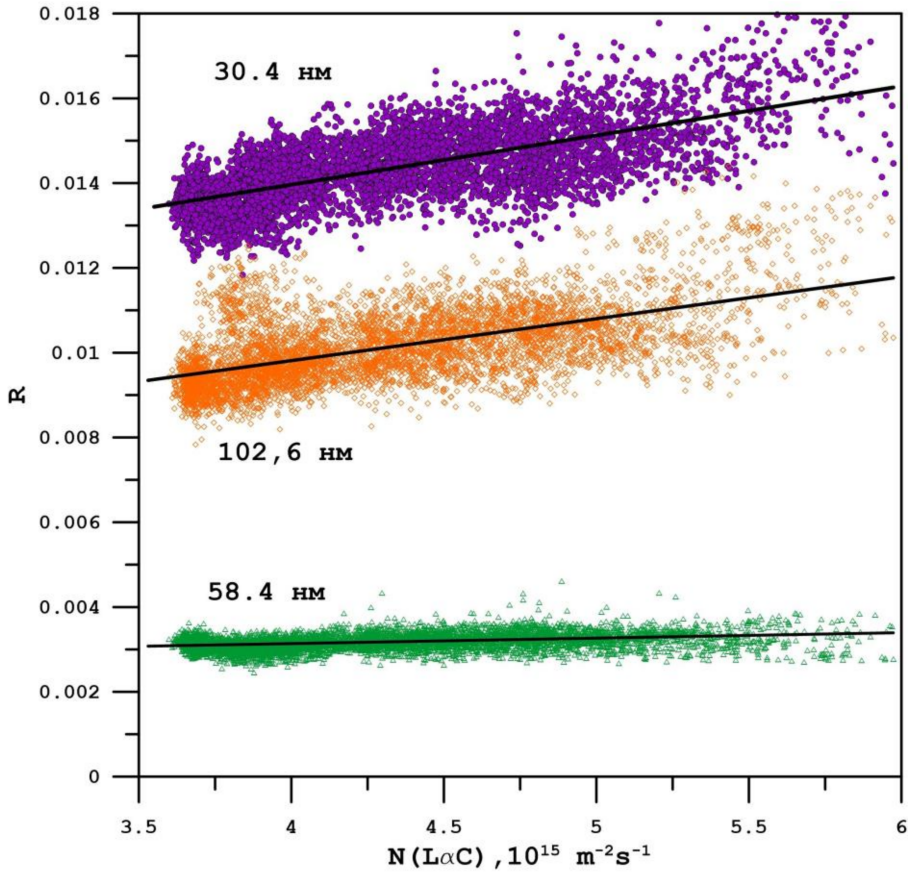

Figure 2. Changes in R_λ values with the level of solar activity, as measured by the N (LaC) index. **Purple**—λ = 30.4 nm; **orange**—λ = 102.6 nm; **green**—λ = 58.4 nm.

The statistical analysis of the dependences obtained makes it possible to determine the coefficients $B0_\lambda$ and $B1_\lambda$ in (2), and to estimate their error also. The resulting set of coefficients, together with Equations (2) and (3), is the model for shortwave radiation. Since the model is based on TIMED satellite data, it will be referred to as EUVT later.

The values of the coefficients of the EUVT model are presented in Table 1 for each wavelength or a wavelength interval. The analysis of the Student's statistical criteria t, which represent a special ratio of the values of the coefficients to the estimation of their errors, showed that their values always exceed the critical values (t = 1.96 for 95% confidence interval), corresponding to the volume n of the studied samples ($n \approx 5400$ observations for each wavelength interval). Thus, all coefficients are statistically significant.

Table 1. Coefficients of the EUVT model.

λ, nm	$B0_\lambda$	$B1_\lambda$	F1	ε,%
5–10	−0.00278	0.00107	7.44	8.2
10–15	−0.00115	0.000584	6.4	6.5
15–20	−0.01062	0.00561	6.46	6.3
20–25	−0.01601	0.00593	7.67	8.6
25.6	−0.00238	0.00170	6.32	5.61
28.4	−0.00178	0.000506	5.69	27.8
25–30	−0.00735	0.004005	7.42	5.9
30.4	0.00921	0.00119	1.93	3.5
30–35	0.00658	0.00383	3.5	4.1
36.8	0.00104	0.000242	1.43	7.3
35–40	−0.00253	0.002215	4.19	6.8
40–45	0.000814	0.000281	2.42	4.5
465	0.000984	−0.00012	2.92	7.3
45–50	0.00232	0.000358	2.45	2.9
50–55	0.000649	0.000589	4.83	3.8
55.4	0.00283	−0.000270	2.88	4.5
58.4	0.00259	0.000136	1.14	4.5
55–60	0.00744	−0.00014	1.06	3.1
61.0	0.000433	0.000329	2.34	6.2
63.0	0.00580	−0.00048	2.52	4
60–65	0.00793	0.00008	1.01	3.4
65–70	0.00221	−0.000036	1.06	2.5
70.3	0.001295	−0.00014	4.65	4.2
70–75	0.00308	−0.00012	1.43	2.4
76.5	0.000721	−0.000086	3.91	5.5
77.0	0.001016	−0.000094	1.8	7.1
78.9	0.00245	−0.00024	3.59	4.1
75–80	0.00956	−0.00065	2.69	2.7
80–85	0.009845	−0.00014	1.06	2.4
85–90	0.01419	0.000988	1.54	2.9
90–95	0.0129	0.000858	1.54	2.8
97.7	0.0121	−0.000097	1.00	7.7
95–100	0.0192	−0.000568	1.08	3.7
102.6	0.00578	0.001005	1.54	5.3
1032	0.00111	0.000142	1.15	8.8
100–105	0.0220	0.002094	1.67	3.2

The estimation of the statistical significance of the regression equation is carried out according to the F—Fisher test, which is the ratio of the initial data variance to the residual variance of the regression equation. The critical value of the Fisher criterion for the above sample size is ~1.02. As it can be seen from the table, in most cases (29 out of 34) the F

value exceeds the critical value. In the opposite case, the coefficient $B1_\lambda$ in Equation (3) can be set equal to 0, and it is reduced to a simple linear dependence on $N_{L\alpha}$.

The modeling accuracy for each line is displayed in Table 1 by the mean relative deviation

$$\varepsilon = (\Sigma \mid N_{\lambda s} - N_{\lambda c} \mid / N_{\lambda s})/n \;\; 100\%, \quad (4)$$

where the indices λs and λccorrespond to the source and model-calculated values at a given wavelength λ, n—the number of measurements. It is seen that the error for most of the wavelength intervals is small and, on average, for the entire spectrum, the value of ε is close to ~5.5%. For example, Figure 3 shows a comparison of the observed values of the flux of quanta $N_{30.4s}$ in the one of the brightest EUV line He II 30.4 nm with the model values of $N_{30.4C}$. It can be seen that the deviations from the calculated values are small. In 75% of cases (3rd quartile of the distribution), they do not exceed 6.5% and only in one case, for a highly variable coronal line Fe XV, the value of ε exceeds 9%.

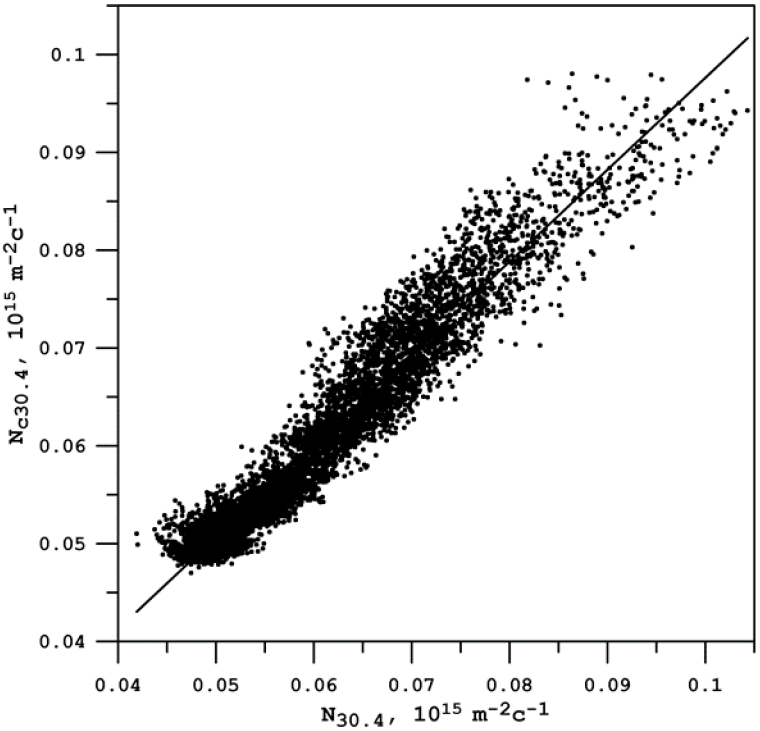

Figure 3. Comparison of the calculated values of the radiation intensity in the 30.4 nm line with the observed ones.

3.2. FUVT Model

For the analysis, we used the daily average data of measurements of the FUV with the SORCE/SOLSTICE apparatus [30] in the 115–242 nm region from the LISIRD database [31]. Measurements corresponding to more than 5500 dates were considered. The web address of the database is http://lasp.colorado.edu/lisird/, accessed on 2 March 2021. The dependence of the photon fluxes in different spectral intervals on the flux in the Lα line was studied at different levels of solar activity. The analysis showed that at all levels of activity, the dependence for any wavelength is close to linear. Examples of analysis results are shown in Figure 4 for two wavelength ranges: 130–131 nm and 200–201 nm, located at the edges of the studied FUV interval.

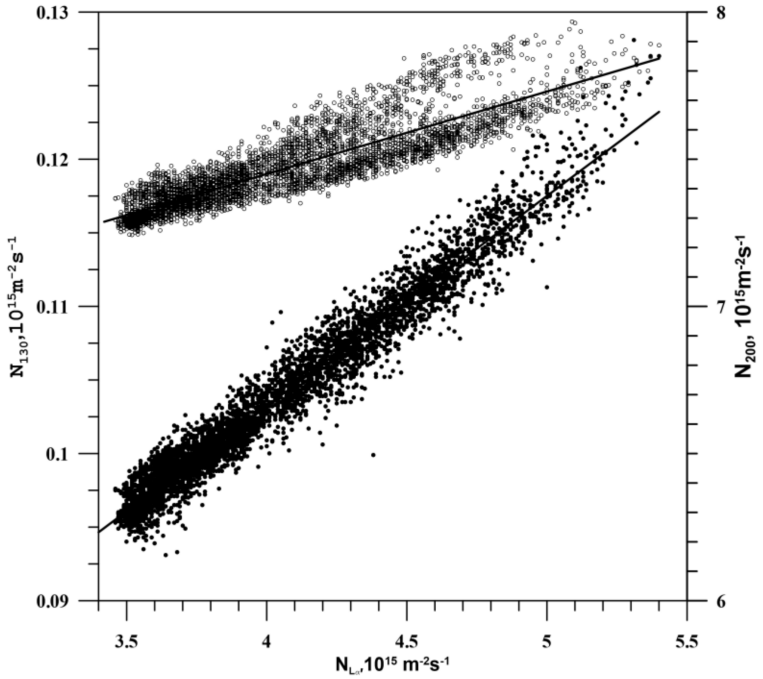

Figure 4. Dependence of photon fluxes in the interval 130–131 nm (dots) and 200–201 nm (circles) on the flux in the Lyman-alpha line.

The figure shows that the deviations of the measurement data from the approximating straight lines are small and do not exceed a few percent. The analysis shows that approximation using higher order polynomials does not lead to any noticeable decrease in the approximation error.

The straight lines in the figure correspond to the linear regression equation

$$N_\lambda = 10^{15} (B0_\lambda + B1\lambda \cdot N_{L\alpha}), \quad (5)$$

where N_λ is in units of $m^{-2}s^{-1}$, and $N_{L\alpha}$ is the photon flux in the Lyman-alpha line in units of 10^{15} $m^{-2}s^{-1}$. The figure shows that the deviations from the regression lines are small and do not exceed a few percent at any level of solar activity. The average deviation ε of the measurement data from the results of the calculation according to the Equation (5) was estimated according to (4). The analysis shows that, when using linear regression, the error ε for all wavelengths does not exceed 2.1%, and the average value of ε over the wavelengths is ~0.8%.

Relation (5) together with the coefficients $B0_\lambda$ and $B1_\lambda$ included in it constitutes the FUVT radiation model. Regression coefficients are determined using standard statistical analysis procedures and are shown in Table 2 for all wavelength intervals λ.

Table 2. Regression coefficients of the FUVT model.

λ, nm	$B0_\lambda$	$B1_\lambda$	λ, nm	$B0_\lambda$	$B1_\lambda$	λ, nm	$B0_\lambda$	$B1_\lambda$
115–116	0.00424	0.001734	158–159	0.0925	0.00868	201–202	7.158	0.265
116–117	0.00948	0.001126	159–160	0.0995	0.00693	202–203	7.158	0.247
117–118	0.0169	0.007721	160–161	0.109	0.00859	203–204	8.283	0.289
118–119	0.01008	0.002265	161–162	0.13	0.01	204–205	9.191	0.329
119–120	0.0110	0.00513	162–163	0.1488	0.01216	205–206	9.526	0.336
120–121	−0.0183	0.027374	163–164	0.1507	0.01537	206–207	9.926	0.349
121–122	−0.00427	0.992896	164–165	0.1582	0.02199	207–208	11.486	0.42
122–123	0.0135	0.006655	165–166	0.281	0.02848	208–209	13.606	0.411
123–124	0.00814	0.004444	166–167	0.2159	0.01392	209–210	20.506	0.417
124–125	0.00564	0.003338	167–168	0.2165	0.02641	210–211	27.206	0.447
125–126	0.00734	0.00249	168–169	0.286	0.01783	211–212	33.276	0.497
126–127	0.00230	0.005296	169–170	0.3831	0.02278	212–213	31.756	0.513
127–128	0.00624	0.001607	170–171	0.4349	0.02845	213–214	28.896	0.457
128–129	0.00536	0.001183	171–172	0.431	0.03058	214–215	41.615	0.606
129–130	0.00296	0.002167	172–173	0.4822	0.03209	215–216	33.975	0.582
130–131	0.0471	0.013437	173–174	0.5085	0.02794	216–217	32.965	0.55
131–132	0.0105	0.001499	174–175	0.6273	0.03411	217–218	32.195	0.55
132–133	0.00734	0.001474	175–176	0.7731	0.04152	218–219	46.084	0.741
133–134	0.00643	0.028979	176–177	0.8574	0.04111	219–220	48.553	0.811
134–135	0.00700	0.001389	177–178	1.0195	0.05595	220–221	48.384	0.768
135–136	0.0181	0.002608	178–179	1.1545	0.05974	221–222	34.175	0.612
136–137	0.0103	0.001943	179–180	1.1435	0.06228	222–223	51.034	0.748
137–138	0.0117	0.001969	180–181	1.4002	0.10246	223–224	65.392	0.924
138–139	0.0124	0.001784	181–182	1.5718	0.14619	224–225	60.333	0.828
139–140	0.00155	0.012505	182–183	1.7263	0.09039	225–226	53.183	0.81
140–141	0.0124	0.008137	183–184	1.8552	0.09679	226–227	36.744	0.776
141–142	0.0176	0.002563	184–185	1.6454	0.0773	227–228	37.764	0.682
142–143	0.0202	0.002513	185–186	1.8893	0.08739	228–229	54.833	0.827
143–144	0.0227	0.003032	186–187	2.1741	0.10726	229–230	46.985	0.637
144–145	0.0223	0.002976	187–188	2.4781	0.11457	230–231	57.213	0.816
145–146	0.0241	0.003187	188–189	2.675	0.12062	231–232	49.234	0.735
146–147	0.0297	0.004032	189–190	2.9138	0.14379	232–233	53.224	0.74
147–148	0.0416	0.00394	190–191	3.1739	0.1337	233–234	44.274	0.692
148–149	0.0413	0.004442	191–192	3.3948	0.14802	234–235	35.815	0.594
149–150	0.0364	0.004313	192–193	3.6647	0.16022	235–236	58.344	0.774
150–151	0.0413	0.004785	193–194	2.9121	0.11178	236–237	44.654	0.731
151–152	0.0441	0.005462	194–195	4.6874	0.20511	237–238	54.764	0.747
152–153	0.0485	0.008556	195–196	4.5824	0.19684	238–239	37.024	0.668
153–154	0.0554	0.009187	196–197	5.2183	0.21155	239–240	47.015	0.546
154–155	0.0700	0.021559	197–198	5.3063	0.21242	240–241	43.466	0.508
155–156	0.0762	0.016004	198–199	5.4134	0.20348	241–242	51.455	0.534
156–157	0.0952	0.011765	199–200	5.8982	0.22616			
157–158	0.0886	0.00961	200–201	6.4461	0.23933			

It should be noted that earlier the procedure for determining the coefficients of the FUV model was carried out using the previous version of the Lα time series [32]. The values in Table 2 correspond to the latest version of the composite Lα.

The model was verified using measurement data with TIMED/SEE equipment, the calibration of which, as well as methods for eliminating degradation effects, are similar to those used in SORCE/SOLSTICE equipment (see, for example, [24,25]). Figure 5 shows the comparison of model calculations results with TIMED measurements for epochs of maximum and minimum solar activity in solar cycle 23.

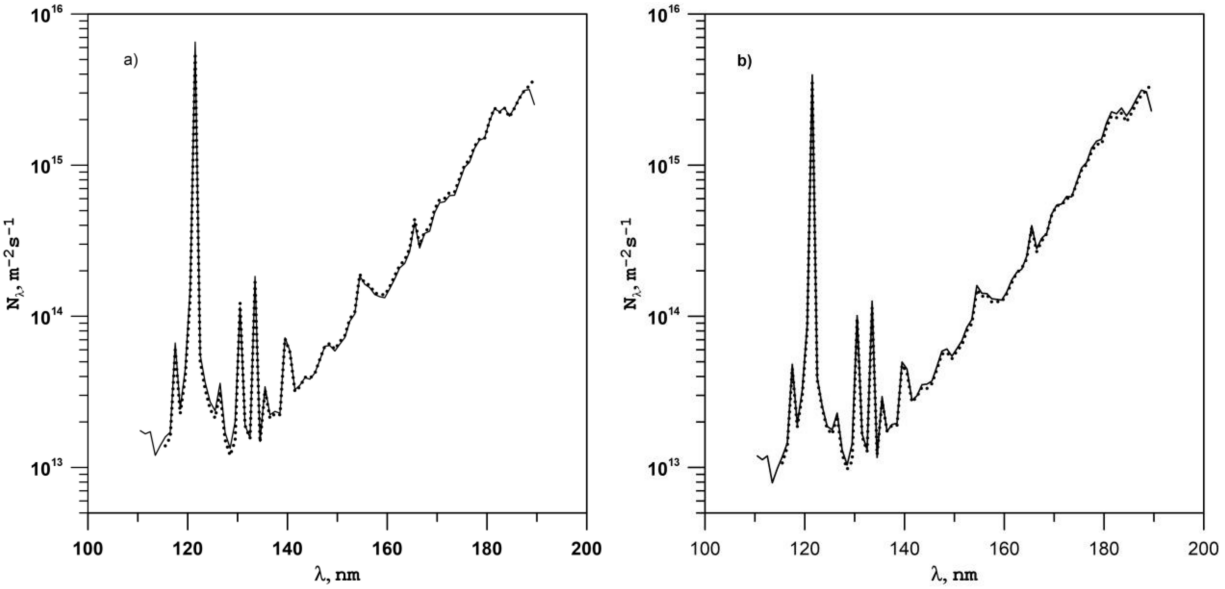

Figure 5. Comparison of model calculations with TIMED/SEE data. (**a**) Near the maximum of activity, 21 February 2002, (**b**) Near the minimum of activity, 21 February 2009. Solid line—measurement data, dashed line—model calculation.

It can be seen that for the entire wavelength range of 115–190 nm, the results of model calculations practically coincide with measurements at both high and low solar activity. It should be noted that the level of high activity falls on the period when measurements at the SORCE, according to which the model has been developed, have not yet been carried out. It can be assumed that the model adequately describes the changes in the FUV spectrum at any level of solar activity and in any solar cycle.

4. Discussion

When using the EUVT model to calculate ionization rates and characteristics of the photoelectron spectrum, one should have an idea of its differences from other models of the EUV spectrum. Since the EUVAC model [15] is often used for these purposes, it is advisable to compare the calculations for this model with the corresponding results of the proposed model. Let us first consider the changes in the value of the total radiation flux N_{tot} in the region of 10–105 nm, which determines the ionization rate at the heights of the F1 and F2 layers. In Figure 6 the results of calculations of N_{tot} daily values are presented for the period 2002–2018. The input parameters for the EUVAC model are the radio flux at 10.7 cm and its average value F10.7A for 81 days. If the data were omitted, the F10.7 values were calculated from the sunspot numbers W (version 2).

The Figure 6 shows that the EUVT model gives systematically higher values than the EUVAC model. The ratio of the results is represented by line 3. The average value of the ratio is 1.37. Thus, it can be expected that when using a model based on modern data on EUV radiation, ionization rates in model calculations of the ionosphere will increase by almost ~40%, which will accordingly affect the parameters of the ionosphere.

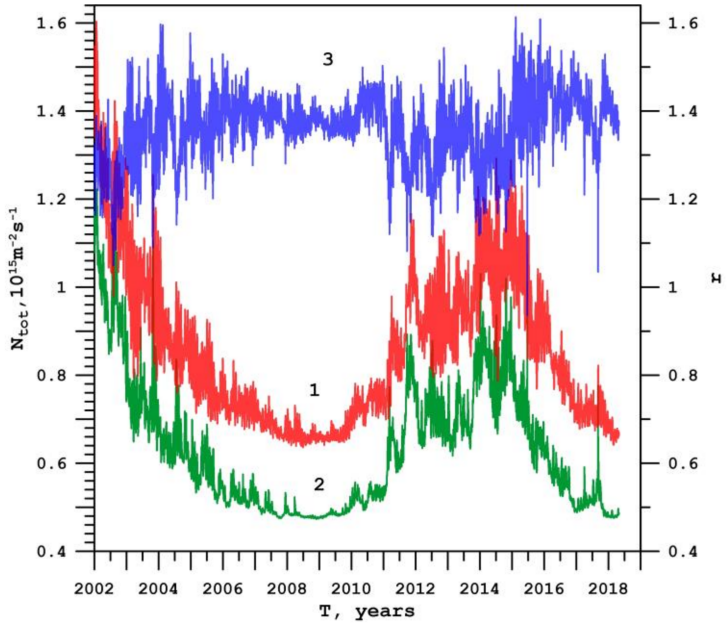

Figure 6. Time variations of the total flux of EUV radiation over 23–24 activity cycles according to calculations using the EUVT (**Line 1**) and EUVAC (**Line 2**) models. (**Line 3**)—their ratio r.

However, the magnitude of the excess is not the same for different parts of the spectrum. Figure 7 represents the results of model calculations for fluxes in the lines of 30.4 nm (lines 1 and 2) and 102.6 nm (lines 3 and 4). Blue lines correspond to the EUVAC model, and red the EUVT model.

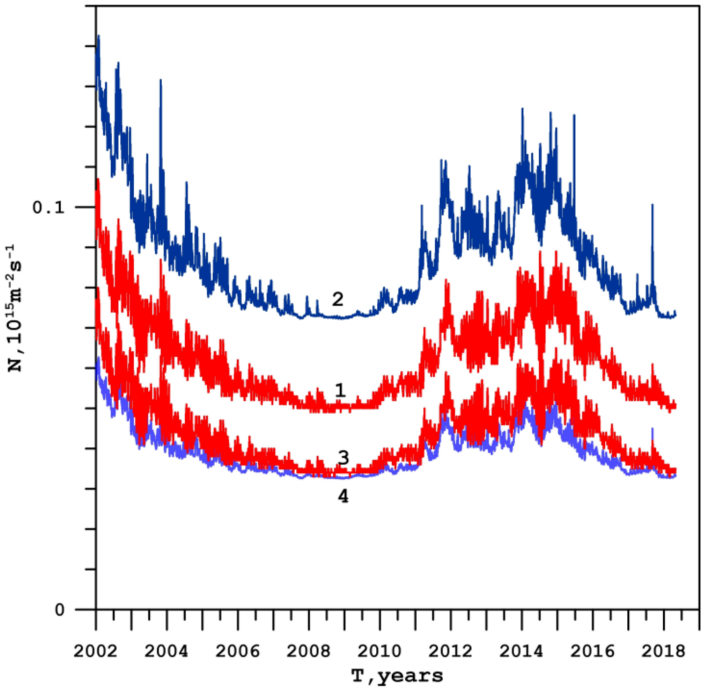

Figure 7. Time variations in the 23–24 activity cycles of individual lines of the EUV region. 1, 2—30.4 nm, 3. 4—102.6 nm. **Blue** lines—EUVAC, **Red**—EUVT.

It can be seen that in line 30.4 EUVAC is always higher than EUVT (by ~30% on average). This fact will affect the modeling of the F-layer. On the contrary, for the 102.6 nm line, calculations by the EUVT model give an excess over EUVAC by an average of ~12%. This spectral line (along with the CIII 97.7 nm line) gives the main contribution to the

ionization of the ionospheric E layer, i.e., when modeling the ionosphere, both models may give approximately the same results for the E-layer. Thus, when calculating the parameters of the ionosphere at different altitudes, the use of EUVT model for ionospheric calculations can lead to results, that contradict to those obtained using EUVAC.

The FUVT model makes it possible to obtain the values of the radiation fluxes in all parts of the spectrum of the considered interval $115 \leq \lambda \leq 242$ nm. In this case, not only the data of current measurements of the input parameter NLα can be used, but also archival data or its model estimates based on some other data, for example, according to the solar radio emission index F10.7 or according to the data on the critical frequencies of the E layer of the ionosphere [6]. Such estimates are important, for example, when planning long-term space experiments. Figure 8 shows the model spectra calculated for the maximum (solid line) and minimum (dashed line) $N_{L\alpha}$ values given in the LISIRD database for the period from 1947 to 2018 (respectively, $N_{L\alpha}$ = 3.31 1015 $m^{-2}s^{-1}$ in 2018 and 7.12 10^{15} $m^{-2}s^{-1}$ in 1947).

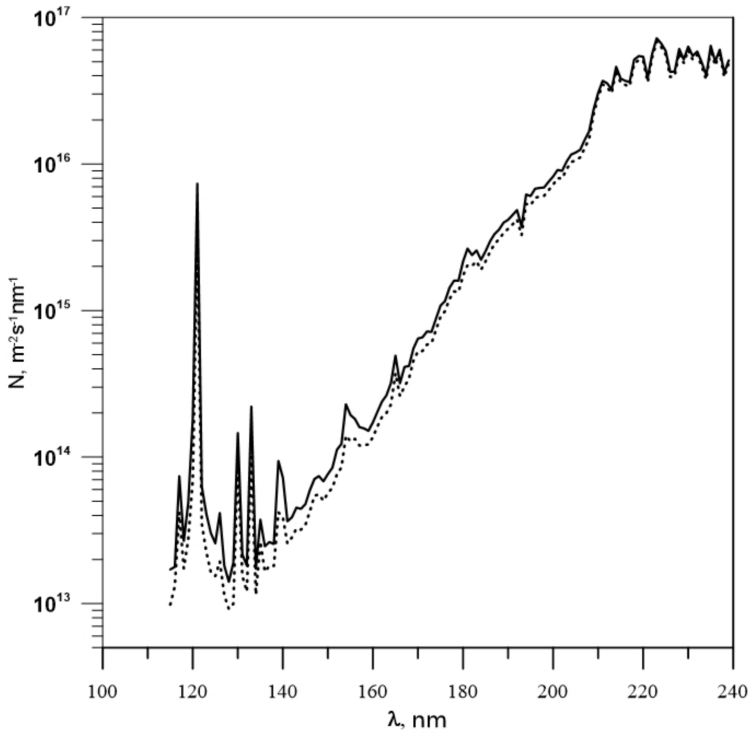

Figure 8. Model spectra for extreme values of the $N_{L\alpha}$ index.

It can be seen from the figure that when the transition occurs from low solar activity to high activity, the FUV fluxes weakly differ in the spectral region $\lambda > 210$ nm. The changes increase markedly when going to shorter wavelengths. It is possible to estimate the maximum values of V variability (the ratio of radiation fluxes for the maximum and minimum levels of solar activity at a given wavelength) from the archived LISIRD data. The results of model calculations of the variability of the FUV fluxes at different wavelengths are shown in Figure 9.

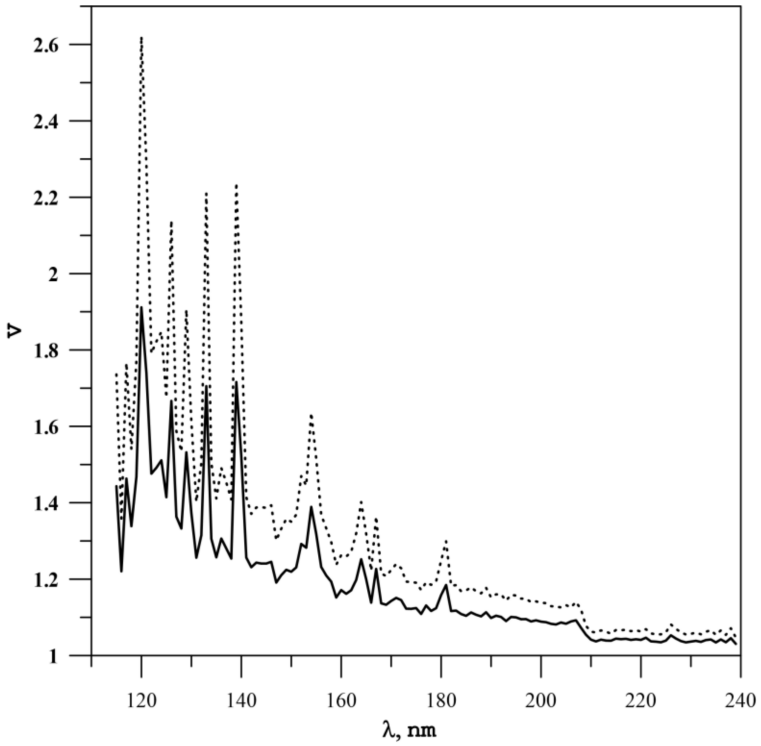

Figure 9. Variability of the FUV spectrum depending on the wavelength. The dotted line is for extreme daily values, the solid line is for extreme $N_{L\alpha}$ values, averaged over 3 solar revolutions.

The dotted line in Figure 9 corresponds to the $N_{L\alpha}$ values for 1947–2018. In view of the inertia of the processes in the upper atmosphere, individual extreme values occurring at relatively short (one or several days) time intervals are hardly advisable to use in model calculations or estimates of the parameters of the upper atmosphere. The solid line in Figure 9 corresponds to the extreme values of the time series obtained by calculating the moving average for three solar revolutions (81 days) of daily values of $N_{L\alpha}$ (respectively, $N_{L\alpha} = 3.5 \cdot 10^{15}$ $m^{-2}s^{-1}$ and $6.1 \cdot 10^{15}$ $m^{-2}s^{-1}$). The use of such a time interval is typical for estimating the state of the ionosphere and the upper atmosphere and leads to more realistic estimates of variations. It can be seen from Figure 9, the intensity of the FUV-radiation at $\lambda < 189$ nm can vary by tens of percent in the activity cycles, but at long wavelengths the changes become insignificant, and at $\lambda > 210$ nm they are only about 4%.

5. Conclusions

1. As a result of comparing the data of the last long-term (23–24 solar cycles) measurements in the TIMED and SORCE projects of the spectra of the extreme (EUV, 10–105 nm) and far (FUV, 115–242 nm) ultraviolet radiation of the Sun as a star, it was revealed that the temporal emission variations were closely related to changes in the emission intensity in the Lα line ($\lambda = 121.6$ nm). The relationship between the intensities in individual spectral lines and intervals with the intensity Lα is close to the quadratic for the EUV region and to the linear one for the FUV. The deviations of the observed values of fluxes from these dependences do not exceed a few percent at any levels of solar activity for 23–24 cycles.
2. The use of the regularities obtained makes it possible to develop the EUVT and FUVT spectrum models, which allow calculating the spectrum in the range of 10–105 nm 115–242 nm for any level of solar activity with an accuracy of several percent. Both models use a single input parameter, the flux of solar radiation quanta in the Lyman-alpha line. Measurements of its intensity have been carried out on satellites for several decades and can now be carried out using simple photometers.

3. The use of the models makes it possible to calculate the fluxes of solar ultraviolet radiation for any levels of solar activity, as well as for any past periods of time, using both the data of current measurements of the flux in the Lα line and the archived data. In the absence of direct measurements, the flux in this line can be reconstructed using archived data on traditional solar indices, i.e., sunspot numbers W, radio flux F10.7 at a wavelength of 10.7 cm, or data on the ionospheric E-layer critical frequencies, as it was proposed by Nusinov [6].

Author Contributions: Conceptualization, A.A.N.; methodology, A.A.N.; investigation, A.A.N., T.V.K.; data curation A.A.N. and V.V.K.; software, A.A.N.; validation, T.V.K. and V.V.K.; writing—original draft preparation, A.A.N., T.V.K. and V.V.K.; writing—review and editing, A.A.N. and V.V.K. All authors have read and agreed to the published version of the manuscript.

Funding: This research received no external funding.

Institutional Review Board Statement: Not applicable.

Informed Consent Statement: Not applicable.

Data Availability Statement: Publicly available datasets were analyzed in this study. This data can be found here: https://lasp.colorado.edu/lisird/ (accessed on 2 March 2021).

Acknowledgments: The authors express their deep gratitude to the team of the Laboratory of Atmospheric and Space Physics (LASP) at the University of Colorado for providing measurements of the extreme ultraviolet radiation of the Sun.

Conflicts of Interest: The authors declare no conflict of interest.

References

1. Okabe, H. *Photochemistry of Small Molecules*; Wiley: Hoboken, NJ, USA, 1978; 431p.
2. Ivanov-Kholodny, G.S.; Mikhailov, A.V. *The Prediction of Ionospheric Conditions*; D. Reidel Publishing Company: Dordrecht, The Netherlands, 1986; Volume 2, p. 16.
3. Pertsev, N.N.; Semenov, A.I.; Shefov, N.N. Empirical model of vertical structure of the middle atmosphere: Seasonal variations and long-term changes of temperature and number density. *Adv. Space Res.* **2006**, *38*, 2465–2469. [CrossRef]
4. Merkel, A.W.; Harder, J.W.; Marsh, D.R.; Smith, A.K.; Fontenla, J.M.; Woods, T.N. The impact of solar spectral irradiance variability on middle atmospheric ozone. *Geophys. Res. Lett.* **2011**, *38*, L13802–L13807. [CrossRef]
5. Solomon, S.C.; Woods, T.N.; Didkovsky, L.V.; Emmert, J.T.; Qian, L. Anomalously low solar extreme-ultraviolet irradiance and thermospheric density during solar minimum. *Geophys. Res. Lett.* **2010**, *37*, L16103. [CrossRef]
6. Nusinov, A.A. Ionosphere as a natural detector for investigations of solar EUV flux variations. *Adv. Space Res.* **2006**, *37*, 426–432. [CrossRef]
7. Chamberlin, P.C.; Woods, T.N.; Crotser, D.A.; Eparvier, F.G.; Hock, R.A.; Woodraska, D.L. New Higher Resolution Solar Extreme Ultraviolet (EUV) Irradiance Results for Solar Cycle Minimum Conditions on April 14, 2008. *Geophys. Res. Lett.* **2009**, *36*, L05102. [CrossRef]
8. Lean, J.L.; Rottman, G.J.; Kyle, H.L.; Woods, T.N.; Hickey, J.R.; Puga, L.C. Detection and parameterization of variations in solar mid and near ultraviolet radiation (200 to 400 nm). *J. Geophys. Res.* **1997**, *102*, 29939–29956. [CrossRef]
9. Lean, J. Evolution of the Sun's Spectral Irradiance since the Maunder Minimum. *Geophys. Res. Lett.* **2000**, *27*, 2425–2428. [CrossRef]
10. Lean, J.; Rottman, G.; Harder, J.; Kopp, G. SORCE contributions to new understanding of global change and solar variability. *Sol. Phys.* **2005**, *230*, 7–53. [CrossRef]
11. Ball, W.T.; Unruh, Y.C.; Krivova, N.A.; Solanki, S.; Harder, J.W. Solar irradiance variability: A six-year comparison between SORCE observations and the SATIRE model. *Astron. Astrophys.* **2011**, *530*, A71. [CrossRef]
12. Yeo, K.L.; Ball, W.T.; Krivova, N.A.; Solanki, S.K.; Unruh, Y.C.; Morrill, J. UV solar irradiance in observations and the NRLSSI and SATIRE-S models. *J. Geophys. Res. Space Physics.* **2015**, *120*, 6055–6070. [CrossRef]
13. Bruevich, E.A.; Nusinov, A.A. The spectrum of shortwave radiation for aeronomical calculations at different levels of solar activity. *Geomagn. Aeron.* **1984**, *24*, 581–585. (In Russian)
14. Nusinov, A.A. Models for prediction of EUV and X-ray solar radiation based on 10.7-cm radio emission. In *Solar Electromagnetic Radiation for Solar Cycle 22*; Donnely, R.F., Ed.; NOAA ERL: Boulder, CO, USA, 1992; pp. 354–359.
15. Richards, P.C.; Fennelly, J.A.; Torr, D.G. EUVAC: A solar EUV flux model for aeronomic calculations. *J. Geophys. Res.* **1994**, *99*, 8981–8992. [CrossRef]
16. Hinteregger, H.E.; Fukui, K.; Gilson, G.R. Observational, reference and model data on solar EUV from measurements on AE-E. *Geophys. Res. Lett.* **1981**, *8*, 1147–1150. [CrossRef]

17. Chamberlin, P.C.; Woods, T.N.; Eparvier, F.G. Flare Irradiance Spectral Model (FISM): Daily component: Algorithms and results. *Space Weather* **2007**, *5*, S07005. [CrossRef]
18. Chamberlin, P.C.; Woods, T.N.; Eparvier, F.G. Flare Irradiance Spectral Model (FISM): Flare component algorithms and results. *Space Weather* **2008**, *6*, S05001. [CrossRef]
19. Tobiska, W.K.; Woods, T.N.; Eparvier, F.G.; Viereck, R.; Floyd, L.; Bower, D.; Rottman, G.J.; White, O.R. The SOLAR2000 empirical solar irradiance model and forcast tool. *J. Atmos. Sol. Terr. Phys.* **2000**, *62*, 1233–1250. [CrossRef]
20. Heath, D.F.; Schlesinger, B.M. The Mg 280 nm doublet as a monitor of changes in the solar ultraviolet irradiance. *J. Geophys. Res.* **1986**, *91*, 8672–8682. [CrossRef]
21. Tobiska, W.K.; Bouwer, S.D.; Bowman, B.R. The development of new solar indices for use in thermospheric density modeling. *J. Atmos. Sol. Terr. Phys.* **2007**, *70*, 803–819. [CrossRef]
22. Lovric, M.; Tosone, E.; Pietropaolo, E.; Del Moro1, D.; Giovannelli, L.; Cagnazzo, C.; Berrilli, F. The dependence of the [FUV-MUV] colour on solar cycle. *J. Space Weather Space Clim.* **2017**, *7*, 8. [CrossRef]
23. Snow, M.; Weber, M.; Machol, J.; Viereck, R.; Richard, E. Comparison of Magnesium II core-to-wing ratio observations during solar minimum 23/24. *J. Space Weather Space Clim.* **2014**, *4*, 6. [CrossRef]
24. Woods, T.N. Recent advances in observations and modeling of the solar ultraviolet and X-ray spectral irradiance. *Adv. Space Res.* **2008**, *42*, 895–902. [CrossRef]
25. Woods, T.N.; Eparvier, F.G.; Harder, J.; Snow, M. Decoupling Solar Variability and Instrument Trends using the Multiple Same-Irradiance-Level (MuSIL) Analysis Technique. *Sol. Phys.* **2018**, *293*, 21. [CrossRef]
26. Schmidtke, G. Extreme ultraviolet spectral irradiance measurements since 1946. *Hist. Geo Space Sci.* **2015**, *6*, 3–22. [CrossRef]
27. Kazachevskaya, T.V.; Nusinov, A.A.; Katyushina, V.V.; Svidsky, P.M.; Gonjukh, D.A. Variability of Extreme Ultraviolet Fluxes at Various Timescales as Measured Onboard the CORONAS Space Mission (SUFR-SP-K and VUSS-L Experiments). In *The Coronas-F Space Mission: Key Results for Solar Terrestrial Physics (Astrophysics and Space Science Library (400))*; Kuznetsov, V.D., Ed.; Springer: Berlin/Heidelberg, Germany, 2014; 495p.
28. Woods, T.N.; Eparvier, F.G.; Bailey, S.M.; Chamberlin, P.C.; Lean, J.; Rottman, G.J.; Solomon, S.C.; Tobiska, W.K.; Woodraska, D.L. The Solar EUV Experiment (SEE): Mission overview and first results. *J. Geophys. Res.* **2005**, *110*, A01312. [CrossRef]
29. Machol, J.; Snow, M.; Woodraska, D.; Woods, T.; Viereck, R.; Coddington, O. An Improved Lyman-Alpha Composite. *Earth Space Sci.* **2019**, *6*, 2263–2272. [CrossRef]
30. Sparn, T.P.; Rottman, G.; Woods, T.N.; Boyle, B.D.; Kohnert, R.; Ryan, S.; Davis, R.; Fulton, R.; Ochs, W. The SORCE spacecraft and operations. *Sol. Phys.* **2005**, *230*, 71–89. [CrossRef]
31. Dewolfe, W.A.; Wilson, A.; Lindholm, D.M.; Pankratz, C.K.; Snow, M.A.; Woods, T.N. Solar Irradiance Data Products at the LASP Interactive Solar IRradiance Data Center (LISIRD). *AGU* **2010**, *2010*, GC21B-0881.
32. Nusinov, A.A.; Kazachevskaya, T.V.; Katyushina, V.V. A Model of Fluxes of Solar Extreme Ultraviolet Irradiance. *Geomagn. Aeron.* **2019**, *59*, 265–271. [CrossRef]